

November 17, 2018

QCD motivated approach to soft interactions at high energies: nucleus-nucleus and hadron-nucleus collisions

E. Gotsman^{*}, A. Kormilitzin[†], E. Levin[‡] and U. Maor[§]

*Department of Particle Physics, School of Physics and Astronomy
Raymond and Beverly Sackler Faculty of Exact Science
Tel Aviv University, Tel Aviv, 69978, Israel*

ABSTRACT: In this paper we consider nucleus-nucleus and hadron-nucleus reactions in the kinematic region: $g A^{1/3} G_{3P} \exp(\Delta Y) \approx 1$ and $G_{3P}^2 \exp(\Delta Y) \approx 1$, where G_{3P} is the triple Pomeron coupling, g is the vertex of Pomeron nucleon interaction, and $1 + \Delta_P$ denotes the Pomeron intercept. We find that in this kinematic region the traditional Glauber-Gribov eikonal approach is inadequate. We show that it is necessary to take into account inelastic Glauber corrections, which can not be expressed in terms of the nucleon-nucleon scattering amplitudes. In the wide range of energies where $\alpha'_P Y \ll R_A^2$, the scattering amplitude for the nucleus-nucleus interaction, does not depend on the details of the nucleon-nucleon interaction at high energy. In the formalism we present, the only (correlated) parameters that are required to describe the data are Δ_P , G_{3P} and g . These parameters were taken from our description of the nucleon-nucleon data at high energies [1]. The predicted nucleus modification factor is compared with RHIC Au-Au data at $W = 200 \text{ GeV}$. Estimates for LHC energies are presented and discussed.

KEYWORDS: Soft Pomeron, Glauber approach, inelastic screening corrections, nucleus modification factor, Pomeron interactions.

PACS: 13.85.-t, 13.85.Hd, 11.55.-m, 11.55.Bq

^{*}Email: gotsman@post.tau.ac.il.

[†]Email: andrey1@post.tau.ac.il.

[‡]Email: leving@post.tau.ac.il.

[§]Email: maor@post.tau.ac.il.

1. Introduction	1
2. Equations for nucleus-nucleus collisions	2
2.1 MPSI approach	3
2.2 The complete set of equations	6
2.3 MPSI solution	8
3. Equations for hadron-nucleus collisions	9
4. Main formulae	10
5. Comparison with the experimental data and predictions	12
5.1 Nucleus-nucleus collisions	12
5.2 Hadron-nucleus collisions	14
6. Conclusions	16

1. Introduction

The main goal of this paper is to generalize our approach to soft interactions developed in Ref. ^[GLMM]_[1], to nucleus-nucleus and hadron-nucleus interactions. This approach is based on two main assumptions that provide a natural bridge to the high density QCD approach (see Refs. ^[BFKL, LI, GLR, MUQT, MV, B, K, JIMWLK]_[2-9]). i) $\alpha'_P = 0$; and ii) All Pomeron-Pomeron interactions can be constructed from triple Pomeron vertices through Fan diagrams.

Based on the above two assumption, we have analyzed in Ref. ^[GLMM]_[1] the available data on $p-p$ and $\bar{p}-p$ soft scattering so as to determine the soft Pomeron features. We obtain:

- 1) $\Delta_P = 0.35$.
- 2) $\alpha'_P = 0.012$. This fitted value supports our input assumption.
- 3) The value of the triple Pomeron vertex coupling $G_{3P} = \gamma \Delta_P$ is small (the fitted $\gamma = 0.0242$).
- 4) Note that Pomeron-hadron (and Regge-hadron) interactions are treated in this approach phenomenologically.

To summarize: The data analysis ^[GLMM] [11] confirms our input assumptions and leads to a natural matching between the soft Pomeron and the pQCD hard Pomeron. Indeed $\Delta_P \approx \alpha_S$, $\gamma \approx \alpha_S^2$ and $\alpha'_P \ll 1$.

In section 2 we derive the main equations governing nucleus-nucleus scattering at high energy. To this end we define the kinematic regions in which our formalism is applicable,

$$g A^{1/3} G_{3P} \exp(\Delta Y) \approx 1 \text{ and } G_{3P}^2 \exp(\Delta Y) \approx 1. \quad (1.1) \quad \boxed{\text{I1}}$$

$1 + \Delta_P$ denotes the intercept of the soft Pomeron, g is the vertex coupling of the Pomeron-nucleon interaction and G_{3P} is the vertex coupling of the triple Pomeron interaction. As we shall see, the kinematic region defined by Eq. (I.1) is wider than the kinematic region relevant to hadron-hadron scattering. Consequently, we have to go beyond the traditional Glauber-Gribov eikonal approach. The result we obtain suggests that it is necessary to take into account the inelastic Glauber correction which can not be expressed in terms of the nucleon-nucleon scattering amplitudes. In the wide range of energies where $\alpha'_P Y \ll R_A^2$, the scattering amplitude for the nucleus-nucleus interaction does not depend on the details of the nucleon-nucleon interaction at high energy. In the formalism we present, the only (correlated) parameters that we need to know are Δ_P , α'_P , G_{3P} and g . Δ_P , G_{3P} and g were obtained from the data analysis of proton-proton soft scattering ^[GLMM] [11]. Our basic dynamical assumption is that $\alpha'_P = 0$, which is supported by the fitted value of $\alpha'_P = 0.012$ obtained in Ref. ^[GLMM] [11]. Since the fitted values of G_{3P} and α'_P are small, Eq. (I.1) is valid over a wide range of energies, including the LHC energy. For the sake of completeness, we discuss in section 3 the main equations for hadron-nucleus interactions that have been derived in the kinematic region of Eq. (I.1) in Refs. ^[SCHW,BGLM] [11, 12]. In section 4 we adjust the general formulae of sections 3 and 4 to the specific approach of Ref. ^[GLMM] [11]. Section 5 is devoted to a comparison of our results with the experimental data, mostly on the nuclear modification factor in the RHIC range of energies. Predictions for LHC energies are presented and discussed. In the conclusions we reflect on the physical meaning of our approach and its relation to the Color Glass Condensate (CGC) model ^[MY] [6].

2. Equations for nucleus-nucleus collisions

In the framework of the Pomeron Calculus ^[GRIBT] [10] (see also Refs. ^[COL,SOFT,LEREG] [13–15]) there are two different kinematic domains where one can develop a theoretical approach for nucleus-nucleus scattering.

In the first domain we consider

$$\begin{aligned} g_1 g_2 \int d^2 b' d^2 b'' S_{A_1}(b'') S_{A_2}(\vec{b} - \vec{b}') P(Y, \vec{b}'' - \vec{b}') &= g_1 g_2 \int d^2 b'' P(Y, b'') \int d^2 b' S_{A_1}(b') S_{A_2}(\vec{b} - \vec{b}') \quad (2.1) \quad \boxed{\text{KR1}} \\ &\propto g_1 g_2 A_1^{1/3} A_2^{1/3} (R_{A_1}^2 + R_{A_2}^2) e^{\Delta_P Y} \approx 1; \\ g_i S_{A_i}(b) G_{3P} e^{\Delta_P Y} &\propto g_i G_{3P} A_i^{1/3} e^{\Delta_P Y} \ll 1; \quad G_{3P}^2 e^{\Delta_P Y} \ll 1. \end{aligned}$$

In this kinematic region the main contribution stems from the diagrams of Fig. ^[glset] 1. Summing these diagrams, we obtain the Glauber-Gribov eikonal expressions describing nucleus-nucleus scattering ^[GLAUB,GRIBA] [16, 17]. In this

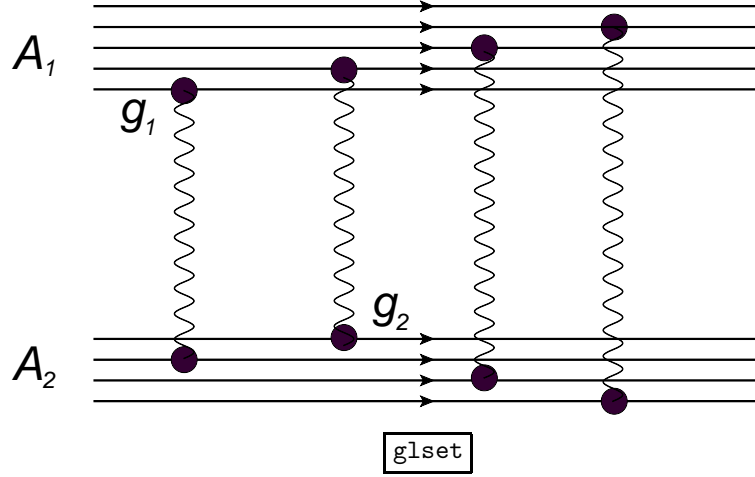


Figure 1: The full set of the diagrams for Glauber-Gribov approach which contribute to the scattering amplitude in the kinematic region of Eq. (2.1) ^{KR1}

approach the nucleus-nucleus amplitude can be derived from the knowledge of the nucleon-nucleon cross section. Specifically, we get

$$\begin{aligned}
 N_{el}(Y; b) &= i \left(1 - \exp \left(-\frac{1}{2} g_1 g_2 \int d^2 b' S_{A_1}(b') S_{A_2}(\vec{b} - \vec{b}') \int d^2 b'' P(Y, b'') \right) \right) \\
 &= \left(1 - \exp \left(-\frac{1}{2} g_1 g_2 \int d^2 b' S_{A_1}(b') S_{A_2}(\vec{b} - \vec{b}') e^{\Delta_Y} \right) \right). \quad (2.2) \quad \boxed{\text{GG}}
 \end{aligned}$$

In the second kinematic region

$$\begin{aligned}
 g_1 g_2 \int d^2 b' d^2 b'' S_{A_1}(b'') S_{A_2}(\vec{b} - \vec{b}') P(Y, \vec{b}'' - \vec{b}') &= g_1 g_2 \int d^2 b'' P(Y, b'') \int d^2 b' S_{A_1}(b') S_{A_2}(\vec{b} - \vec{b}') \quad (2.3) \quad \boxed{\text{KR2}} \\
 &\propto g_1 g_2 A_1^{1/3} A_2^{1/3} (R_{A_1}^2 + R_{A_2}^2) e^{\Delta_{PY}} > 1; \\
 g_i S_{A_i}(b) G_{3P} e^{\Delta_{PY}} &\propto g_i G_{3P} A_i^{1/3} e^{\Delta_{PY}} \approx 1; \quad G_{3P}^2 e^{\Delta_{PY}} \ll 1,
 \end{aligned}$$

it is necessary to consider the the more complicated set of diagrams presented in Fig. 2. ^{netset} We conclude that the knowledge of the nucleon-nucleon amplitude is not sufficient to enable a calculation of nucleus-nucleus scattering. In addition to the above, we also need to know the structure of the Pomeron-Pomeron interactions, so as to tackle the problem of the summation of these diagrams. In Fig. 2 ^{netset} we assume that only the triple Pomeron vertex contributes to multi Pomeron interactions.

As stated, the main goal of this paper is to calculate the nucleus-nucleus amplitude in the kinematic region of Eq. (2.3). ^{KR2} We start with the MPSI approach ^{MPSI} [18].

2.1 MPSI approach

The MPSI approach is based on the observation that for a Pomeron with a intercept larger than 1, i.e. $\Delta_P > 0$, the main diagrams of interest have the form of Fig. 3 ^{mpsiset} with an arbitrary y which is of the order of

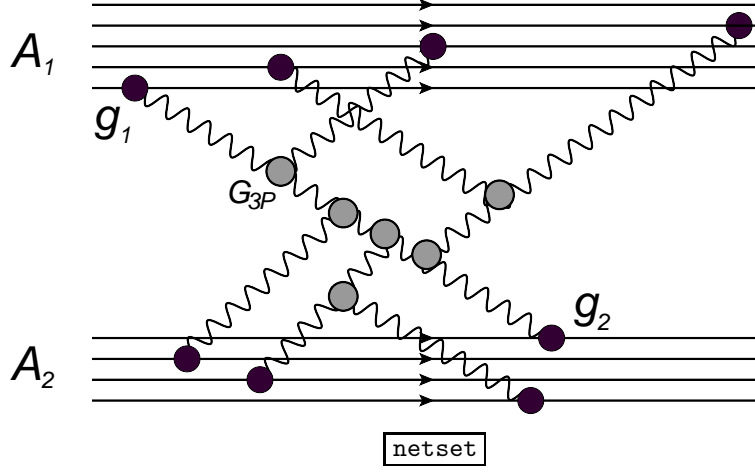


Figure 2: The full set of the diagrams that contribute to the scattering amplitude for the kinematic region Eq. (2.3). KR2

Y . We have discussed this approach in our previous publication [11, 19]. The method of calculating the sum of Fig. 3 diagrams is based on t -channel unitarity adjusted [18] to the summation of Pomeron diagrams. GLMM, LMP

The general formula has the form

$$\begin{aligned}
 N_{el}^{MPSI}(Y) &= \sum_{n=1}^{\infty} (-1)^{n+1} \frac{1}{n!} \gamma^n \frac{\partial^n N^{MFA}(Y-y, \gamma_R^p)}{\partial^n \gamma_R^p} \Big|_{\gamma_R^p=0} \frac{\partial^n N^{MFA}(y, \gamma_R^t)}{\partial^n \gamma_R^t} \Big|_{\gamma_R^t=0} \\
 &= 1 - \left\{ \exp \left(-\gamma \frac{\partial}{\partial \gamma_R^p} \frac{\partial}{\partial \gamma_R^t} \right) N^{MFA}(Y-y, \gamma_R^p) N^{MFA}(y, \gamma_R^t) \right\} \Big|_{\gamma_R^p=0; \gamma_R^t=0} .
 \end{aligned} \tag{2.4} \quad \text{MPSI}$$

$\gamma_R^{p,t}$ are related to projectile and target, respectively, and γ is the amplitude for 'wee' partons (colorless dipoles in QCD) scattering at low energies. N^{MFA} denotes the amplitude, which for a nucleus has the form

$$N_{A_i}^{MFA}(y, b) = 1 - \exp(-\tilde{g}_i S_{A_i}(b) N_N^{MFA}). \tag{2.5} \quad \text{MPSI1}$$

Here, N_N^{MFA} denotes the sum of Fig. 4 diagrams where $\tilde{g}_1 \tilde{g}_2 \gamma = g_1 g_2$. In the case of $\alpha'_{IP} \ll 1$, i.e. for energies $\alpha'_{IP} Y < R_A^2$, this sum is

$$N_N^{MFA} = \frac{\gamma_R e^{\Delta_F(Y-y)}}{1 + \gamma_R e^{\Delta_F(Y-y)}}, \tag{2.6} \quad \text{MPSI2}$$

where γ_R denotes the scattering amplitude at low energy of the 'wee' parton (colorless dipole in QCD) with the target.

Using a generating function for Laguerre polynomials (see Ref. [20] formula 8.973(1)), RY

$$(1-z)^{-\alpha-1} \exp\left(\frac{xz}{z-1}\right) = \sum_{n=0}^{\infty} L_n^\alpha(x) z^n, \tag{2.7} \quad \text{MPSI3}$$

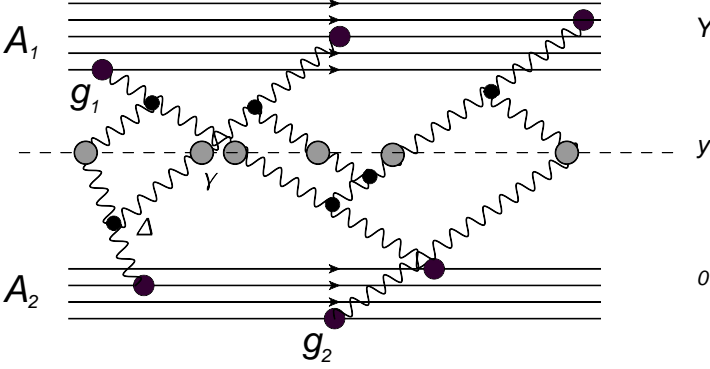


Figure 3: The set of diagrams that contribute to the scattering amplitude in the MPSI approximation in the kinematic region Eq. (2.3).

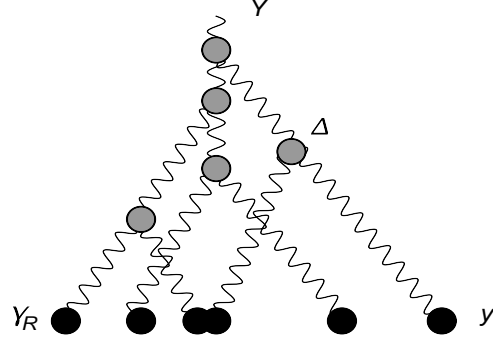


Figure 4: The set of fan diagrams that contribute to N_N^{MFA} .

we obtain for Eq. (2.6)

$$N^{MFA}(Y-y; \gamma_R) = - \sum_{n=1}^{\infty} L_n^{-1}(\tilde{g}_i) \left(-\gamma_R e^{\Delta_P(Y-y)} \right)^n. \quad (2.8) \quad \text{MPSI4}$$

For simplicity we have omitted the b dependence which is easy to include, as each \tilde{g}_i should be multiplied by $S_{A_i}(b)$.

Using Eq. (2.7) and Eq. (2.4) we have for the scattering amplitude,

$$N^{MFA}(Y) = \sum_{n=0}^{\infty} n! L_n^{-1}(\tilde{g}_i) L_n^{-1}(\tilde{g}_k) \left(-\gamma e^{\Delta_P Y} \right)^n. \quad (2.9) \quad \text{MPSI5}$$

Introducing $n! = \int_0^\infty \xi^n e^{-\xi} d\xi$, we can re-write Eq. (2.9) in the form

$$N^{MFA}(Y;) = \int_0^\infty d\xi e^{-\xi} d \sum_{n=0}^{\infty} L_n^{-1}(\tilde{g}_i) L_n^{-1}(\tilde{g}_k) \left(-\xi \gamma_0 e^{\Delta_P Y} \right)^n. \quad (2.10) \quad \text{MPSI6}$$

$\gamma_0 = G_{3P}/\Delta_P$ is obtained from the data analysis of soft proton-proton scattering [1]. Using formula 8.976(1) of Ref. [20],

$$\sum_{n=0}^{\infty} n! z^n \frac{L_n^\alpha(x) L_n^\alpha(y)}{\Gamma(n+\alpha+1)} = \frac{(xy)^{-\frac{1}{2}\alpha}}{1-z} \exp\left(-z \frac{x+y}{1-z}\right) I_\alpha\left(2 \frac{\sqrt{xy}}{1-z}\right), \quad (2.11) \quad \text{SUML}$$

we derive the final result

$$N_{i,k}^{MFA}(Y) = \int_0^\infty \frac{d\xi}{\xi} e^{-\xi} \frac{(\tilde{g}_i \tilde{g}_k \xi T(Y))^{\frac{1}{2}}}{1 + \xi T(Y)} \exp\left\{-\xi T(Y) \frac{\tilde{g}_i + \tilde{g}_k}{1 + \xi T(Y)}\right\} J_1\left(2 \frac{\sqrt{\tilde{g}_i \tilde{g}_k \xi T(Y)}}{1 + \xi T(Y)}\right), \quad (2.12) \quad \text{MPSI7}$$

where

$$T(Y) = \gamma e^{\Delta_P Y}. \quad (2.13) \quad \text{T}$$

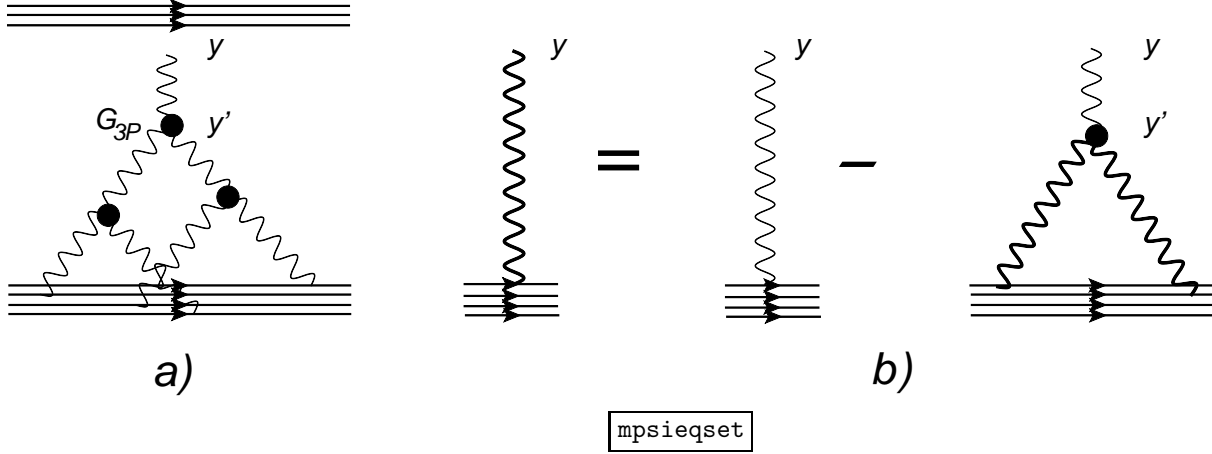


Figure 5: The diagram set that contributes to the scattering amplitude in the approximation in which only a merging of two Pomeron into a single Pomeron has been taken into account in the kinematic region of Eq. (2.3). KR2

Recalling that the function should depend on $\tilde{q}_1 \tilde{g}_2 \gamma$, on $\tilde{q}_1 \gamma$ or on $\tilde{q}_2 \gamma$, one can see that Eq. (2.12) ^{MPSI7} reduces to a simple and elegant formula for the case where we have $\tilde{g}_i T(Y) \sim 1$, $\tilde{g}_i \tilde{g}_i T(Y) > 1$ and $T(Y) \ll 1$. Indeed, after integrating over ξ we get

$$A_{i,k}(Y; b) = 1 - \exp \left\{ - \frac{\tilde{g}_i \tilde{g}_k T(Y)}{1 + T(Y) [\tilde{g}_i + \tilde{g}_k]} \right\}. \quad (2.14) \quad \text{MPSI8}$$

For Eq. (2.14) ^{MPSI8} it is easy to write the expression that takes into account the correct impact parameter behavior. It has the form

$$A(Y; b) = i \left(1 - \exp \left\{ - \frac{1}{2} \int d^2 b' \frac{(\tilde{g}_1 S_{A_1}(\vec{b}')) \tilde{g}_2 S_{A_2}(\vec{b} - \vec{b}') T(Y)}{1 + T(Y) [\tilde{g}_1 S_{A_1}(\vec{b}') + \tilde{g}_2 S_{A_2}(\vec{b} - \vec{b}')] } \right\} \right). \quad (2.15) \quad \text{MPSI91}$$

2.2 The complete set of equations

We start the derivation of the complete set of equations beyond MPSI approximation assuming that the merging of two Pomeron into one Pomeron is equal to zero. In this case we need to sum the ‘fan’ diagrams of Fig. 5-a ^{mpsieqset} which we can do using the following equation (see Fig. 5-b) ^{mpsieqset}

$$G_{MFA}(y) = g_2 e^{\Delta_P y} - G_{3P} \int^y dy' e^{\Delta_P (y-y')} G_{MFA}^2(y'), \quad (2.16) \quad \text{CS1}$$

which can be rewritten in a differential form

$$\frac{dG_{MFA}(y)}{dy} = \Delta_P G_{MFA}(y) - G_{3P} G_{MFA}^2(y'), \quad (2.17) \quad \text{CS2}$$

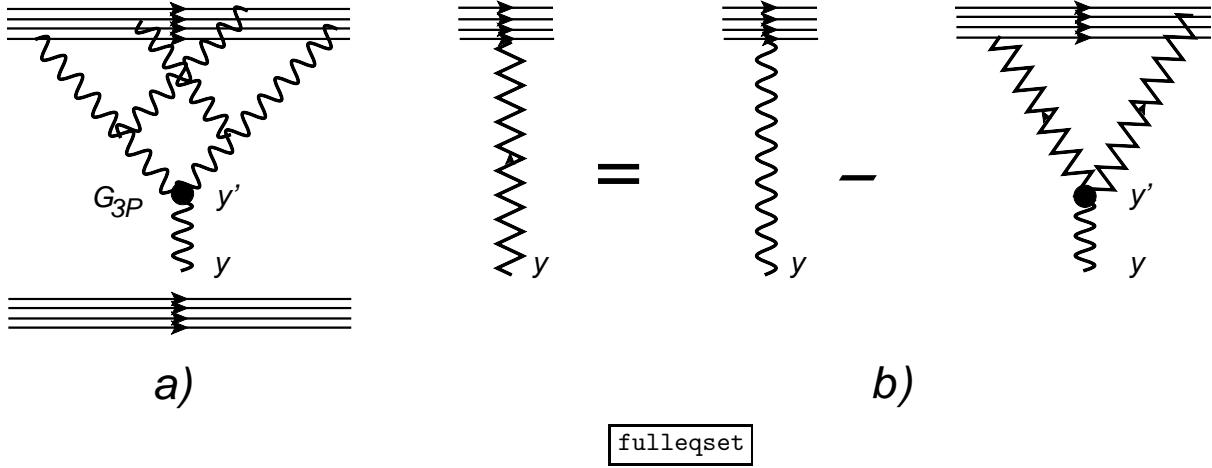


Figure 6: The set of the diagrams that contributes to the scattering amplitude in the approximation in which both the decay of a single Pomeron into two Pomerons, and the merging of two Pomerons into a single Pomeron have been taken into account in the kinematic region of Eq. (2.3). KR2

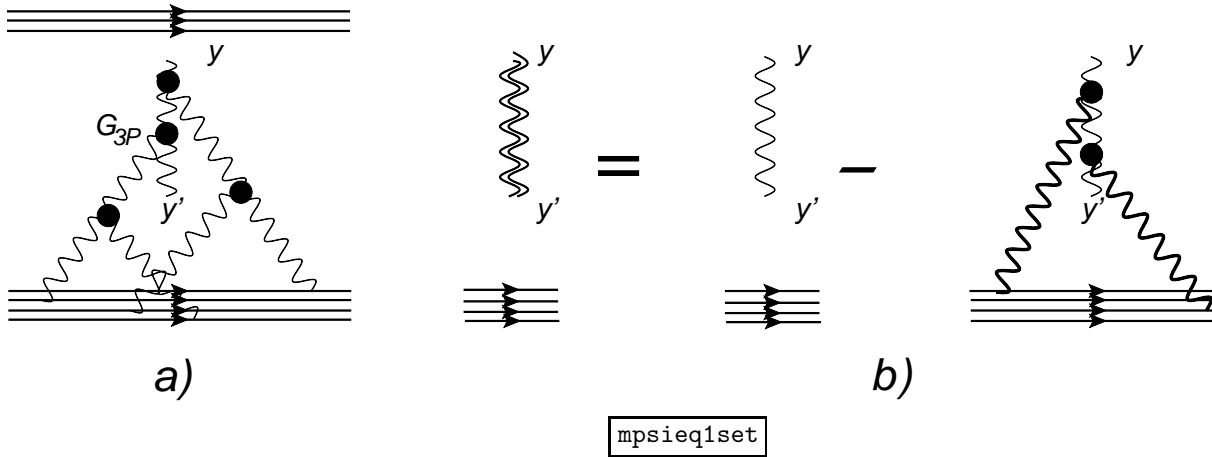


Figure 7: The set of diagrams that contribute to the Green function $G(y, y')$ in the approximation in which only the merging of two Pomerons into a single Pomeron has been taken into account in the kinematic region of Eq. (2.3). KR2

with the initial condition

$$G_{MFA}(y=0) = g_2 S_{A_2} (\vec{b} - \vec{b}'). \quad (2.18) \quad \text{CS3}$$

The solution to this equation is

$$G_{MFA}(y) = \frac{g_2 e^{\Delta_P y}}{1 + g_2 \frac{G_{3P}}{\Delta_P} (e^{\Delta_P y} - 1)}. \quad (2.19) \quad \text{CS4}$$

We denote this solution by a bold wave lines in Fig. fulleqset, Fig. mpsieq1set and Fig. mpsieq1set.

We need to sum the diagrams of Fig. fulleqset to obtain the exact two nuclei irreducible amplitude. We recall that the Glauber-Gribov formula (see Fig. glset) sums all two nuclei reducible diagrams given by the

exchange of a single Pomeron. The equation for the exact amplitude is illustrated in graphic form in Fig. 6-b and has the form

$$G_{exact}(y) = G_{MFA}(Y, y) - G_{3P} \int_y^Y dy' G_{exact}^2(y') G_{MFA}(y', y). \quad (2.20) \quad \boxed{\text{CS5}}$$

The diagrams for $G_{MFA}(y', y)$ are shown in Fig. 7-a and they can be summed using the equation shown in Fig. 7-b. However, for the simple case of a Pomeron with $\alpha'_{\mathbb{P}} = 0$ we can use the property of the propagator for $G_{MFA}(y)$

$$G_{MFA}(y', y) G_{MFA}(y) = G_{MFA}(y'), \quad (2.21) \quad \boxed{\text{CS6}}$$

which leads to

$$G_{MFA}(y', y) = G_{MFA}(y') / G_{MFA}(y). \quad (2.22) \quad \boxed{\text{CS7}}$$

Using this solution we can rewrite Eq. (2.20) in the form

$$G_{exact}(y) = \frac{G_{MFA}(Y)}{G_{MFA}(y)} - G_{3P} \frac{1}{G_{MFA}(y)} \int_y^Y dy' G_{exact}^2(y') G_{MFA}(y'), \quad (2.23) \quad \boxed{\text{CS8}}$$

which can be written in a differential form as

$$\frac{dG_{exact}(y)}{dy} = \frac{d \ln G_{MFA}(y)}{dy} G_{exact}(y) - G_{3P} G_{exact}^2(y). \quad (2.24) \quad \boxed{\text{CS9}}$$

The corresponding initial condition is

$$G_{exact}(y = Y) = g_1 S_{A_1}(b'). \quad (2.25) \quad \boxed{\text{CS10}}$$

Using the solution to Eq. (2.24) we can write the scattering amplitude which will differ from Eq. (2.2) by the replacement $P(Y) \rightarrow G_{exact}(Y, b', \vec{b} - \vec{b}')$. It has the form

$$N_{el}(Y; b) = i \left(1 - \exp \left(-\frac{1}{2} \int d^2 b' G_{exact}(Y; b', \vec{b} - \vec{b}') \right) \right). \quad (2.26) \quad \boxed{\text{GGE}}$$

2.3 MPSI solution

We have not found the general solution to Eq. (2.24), but it is easy to demonstrate that within the MPSI approximation this equation leads to the scattering amplitude of Eq. (2.14). First, we notice that the set of 'fan' diagrams in the MPSI approximation (see Fig. 8) is different from Eq. (2.16) since, starting from rapidity y'' the Pomerons cannot split into two Pomerons. Therefore, the number of Pomerons at $y = y''$ is the same as at $y = 0$. Having this in mind, we obtain a solution for $G_{MFA}(Y, y'')$,

$$G_{MFA}(Y, y'') = \frac{g_1 e^{\Delta_{\mathbb{P}}(Y - y'')}}{1 + \frac{G_{3P} g_2}{\Delta_{\mathbb{P}}} (e^{\Delta_{\mathbb{P}} Y} - 1)}. \quad (2.27) \quad \boxed{\text{SOLMPSI1}}$$

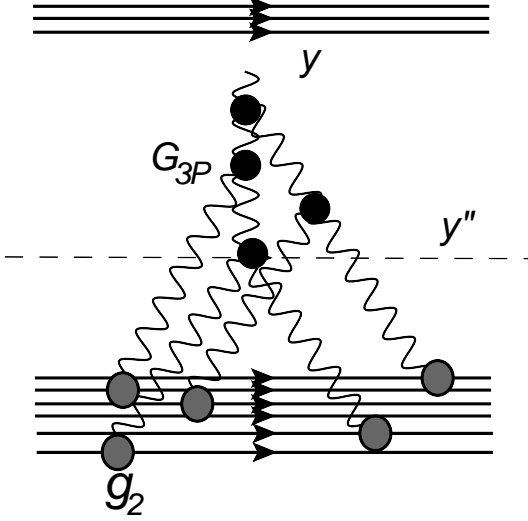


Figure 8: The set of the diagrams that contribute to G_{MFA} in the MPSI approximation.

One can check that this equation sums the diagrams of Fig. 8 by expanding Eq. (2.27) with respect to $\left(\frac{G_{3P} g_2}{\Delta_P} e^{\Delta_P Y}\right)^n$. On the other hand, we can use Eq. (2.4) substituting $N^{MFA}(Y - y'', \gamma_R^p)$ given by Eq. (2.6) and taking $N^{MFA}(y'', \gamma_R^t) = 1 - \exp(-\gamma_R^t e^{\Delta_P y''})$. The second observation is that Eq. (2.24) degenerates to

$$\frac{dG_{exact}(y)}{dy} = \Delta_P G_{exact}(y) - G_{3P} G_{exact}^2(y), \quad (2.28) \quad \text{SOLMP SI2}$$

with the initial condition

$$G_{exact}(y = Y) = G_{MFA}(Y, y''). \quad (2.29) \quad \text{SOLMP SI3}$$

One can see that such a solution has the form

$$G_{exact}(Y) = \frac{g_1 g_2 e^{\Delta_P Y}}{1 + \frac{G_{3P}}{\Delta_P} (g_1 + g_2) e^{\Delta_P Y}}, \quad (2.30) \quad \text{SOLMP SI4}$$

which coincides with Eq. (2.14) since $g_1 g_2 e^{\Delta_P Y} = \tilde{g}_1 \tilde{g}_2 T(Y)$ and $(G_{3P}/\Delta_P)(g_1 + g_2) = (\tilde{g}_1 + \tilde{g}_2) T(Y)$. Substituting Eq. (2.30) into Eq. (2.26) we obtain that Eq. (2.15) presents the scattering amplitude.

3. Equations for hadron-nucleus collisions

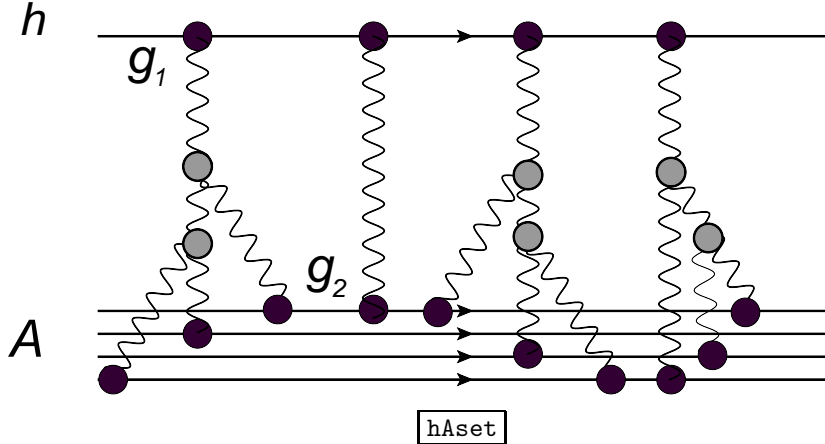


Figure 9: The set of diagrams that contribute to the scattering amplitude of hadron-nucleus scattering in the kinematic region given by Eq. (3.1).

For hadron-nucleus collisions we have only one kinematic region (Eq. (3.1)) in which we calculate the scattering amplitude. This region is similar to the second nucleus-nucleus scattering kinematic region (see

Eq. (2.3).

$$\begin{aligned} g_i S_{A_i}(b) G_{3P} e^{\Delta_{PY}} &\propto g_i G_{3P} A_i^{1/3} e^{\Delta_{PY}} \approx 1; \\ G_{3P}^2 e^{\Delta_{PY}} &\ll 1. \end{aligned} \quad (3.1) \quad \boxed{\text{KRHA}}$$

In this kinematic region, the hadron-nucleus scattering amplitude can be written in an eikonal form in which the opacity Ω is given by sum of the 'fan' diagrams [11] (see Fig. 9).

$$A_{hA}(Y, b) = i \left(1 - \exp \left(-\frac{\Omega_{hA}(Y; b)}{2} \right) \right), \quad (3.2) \quad \boxed{\text{HA1}}$$

with

$$\Omega_{hA}(Y; b) = \frac{\tilde{q}_h \tilde{g} G_{enh}(y) S_A(\vec{b})}{1 + \tilde{g} G_{enh}(y) S_A(\vec{b})}. \quad (3.3) \quad \boxed{\text{HA2}}$$

Using Eq. (3.2) and Eq. (3.3), we obtain that

$$\begin{aligned} \sigma_{tot}^{hA} &= 2 \int d^2b \left(1 - \exp \left(-\frac{\Omega_{hA}(Y; b)}{2} \right) \right); \\ \sigma_{el}^{hA} &= \int d^2b \left(1 - \exp \left(-\frac{\Omega_{hA}(Y; b)}{2} \right) \right)^2; \\ \sigma_{in}^{hA} &= \int d^2b (1 - \exp(-\Omega_{hA}(Y; b))). \end{aligned} \quad (3.4) \quad \boxed{\text{HA3}}$$

The processes of diffractive production have been discussed in Refs. [12, 22].

4. Main formulae

In this paper Eq. (2.15) replaces the Glauber-Gribov eikonal formula to describe the experimental data. However, we need to adjust this formula to our description of hadron-hadron data given in Ref. [11]. In this paper we use two ingredients that were not taken into account in Eq. (2.15):

- 1) A two channel Good-Walker model [21] which is exclusively responsible for low mass diffraction.
- 2) Enhanced Pomeron diagrams that lead to a different Pomeron Green's function. This mechanism is the main contributor to high mass diffraction.

In the two channel model we assume that the observed physical hadronic and diffractive states are written in the form

$$\psi_h = \alpha \Psi_1 + \beta \Psi_2; \quad \psi_D = -\beta \Psi_1 + \alpha \Psi_2, \quad (4.1) \quad \boxed{\text{MF1}}$$

where $\alpha^2 + \beta^2 = 1$. Note that Good-Walker diffraction is presented by a single wave function ψ_D . In our initial approach in which the Pomeron interaction with a nucleus proceeds through an elastic scattering with a single nucleon, we need to replace \tilde{g}_i by $\alpha^2 \tilde{g}_i^{(1)} + \beta^2 \tilde{g}_i^{(2)}$. $\tilde{g}_i^{(k)}$ which denotes the vertex of the

Pomeron interaction with nucleus 1 of the states that have been described by either the wave functions Ψ_1 or Ψ_2 . Since $g_1 = g_2$ we can simplify Eq. (2.15) replacing \tilde{g}_1 and \tilde{g}_2 by $\tilde{g}_1 = \tilde{g}_2 = \tilde{g} = \alpha^2 \tilde{g}^{(1)} + \beta^2 \tilde{g}^{(2)}$. MPSI191

In the framework of our approach we consider $G_{3P}^2 \exp(\Delta_P Y) \ll 1$ and, therefore, we can use the Pomeron's Green function written in the form

$$G(Y) = e^{\Delta_P Y}. \quad (4.2) \quad \text{MF11}$$

In Ref. [1] we sum all enhanced Pomeron diagrams. This leads to the replacement of the 'bare' Pomeron Green function, $G(Y) = \exp(\Delta_P Y)$, by the Green function that sums the enhanced diagrams

$$\gamma G(Y) \longrightarrow G_{enh}(Y) = 1 - \exp\left(\frac{1}{T(Y)}\right) \frac{1}{T(Y)} \Gamma\left(0, \frac{1}{T(Y)}\right). \quad (4.3) \quad \text{MF2}$$

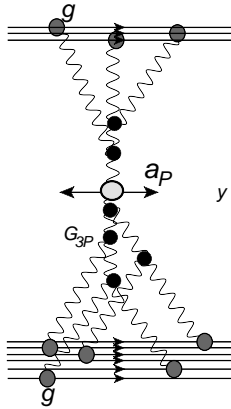
$\Gamma(0, x)$ is the incomplete Gamma function (see 8.350 - 8.359 in Ref. [20]) and $T(Y)$ is given by Eq. (2.13). RY

Finally, we have the main formulae for the total and inelastic nucleus-nucleus cross sections

$$\sigma_{tot}(A_1 + A_2; Y) = 2 \int d^2b \left(1 - \exp \left\{ -\frac{1}{2} \int d^2b' \frac{(\tilde{g} S_{A_1}(\vec{b}')) \tilde{g} S_{A_2}(\vec{b} - \vec{b}') G_{enh}(Y)}{1 + G_{enh}(Y) [\tilde{g} S_{A_1}(\vec{b}') + \tilde{g} S_{A_2}(\vec{b} - \vec{b}')] } \right\} \right); \quad (4.4) \quad \text{MF3}$$

$$\sigma_{in}(A_1 + A_2; Y) = \int d^2b \left(1 - \exp \left\{ - \int d^2b' \frac{(\tilde{g} S_{A_1}(\vec{b}')) \tilde{g} S_{A_2}(\vec{b} - \vec{b}') G_{enh}(Y)}{1 + G_{enh}(Y) \tilde{g} [S_{A_1}(\vec{b}') + S_{A_2}(\vec{b} - \vec{b}')] } \right\} \right). \quad (4.5) \quad \text{MF4}$$

with $\tilde{g} = \alpha^2 \tilde{g}^{(1)} + \beta^2 \tilde{g}^{(2)}$.



Using the AGK cutting rules [23], we obtain the formula for inclusive production (see the Mueller diagrams [24] for the process shown in Fig. 10). The general formula for the inclusive cross section has the form AGK

$$\frac{1}{\sigma_{in}(Y)} \frac{d\sigma}{dy} = a_P \frac{\sigma_{in}^{MFA}(Y - y; A_1) \sigma_{in}^{MFA}(y; A_2)}{\sigma_{in}(Y)}. \quad (4.6) \quad \text{MF5}$$

Using Eq. (2.5) and Eq. (2.6) one obtains MPSI1

$$\sigma_{in}^{MFA}(y; A) = \int d^2b \frac{\tilde{g} G_{enh}(y) S_A(\vec{b})}{1 + \tilde{g} G_{enh}(y) S_A(\vec{b})}. \quad (4.7) \quad \text{MF6}$$

Figure 10: The set of the diagrams that contribute to the inclusive production of hadron in ion-ion collisions. incl

5. Comparison with the experimental data and predictions

5.1 Nucleus-nucleus collisions

The new results presented in this paper are given in Eq. (4.4)^{MF3} and Eq. (4.5)^{MF4}. As noted they can be re-written in a Glauber-like form,

$$\sigma_{tot}(A_1 + A_2; Y) = 2 \int d^2b \left(1 - \exp \left\{ -\frac{1}{2} \int d^2b' \frac{(\sigma_{tot}^{NN} S_{A_1}(\vec{b}')) S_{A_2}(\vec{b} - \vec{b}') G_{enh}(Y)}{1 + G_{enh}(Y) [\tilde{g} S_{A_1}(\vec{b}') + \tilde{g} S_{A_2}(\vec{b} - \vec{b}')] } \right\} \right); \quad (5.1) \quad \boxed{\text{CEP1}}$$

$$\sigma_{in}(A_1 + A_2; Y) = \int d^2b \left(1 - \exp \left\{ - \int d^2b' \frac{(\sigma_{in}^{NN} S_{A_1}(\vec{b}')) S_{A_2}(\vec{b} - \vec{b}') G_{enh}(Y)}{1 + G_{enh}(Y) \tilde{g} [S_{A_1}(\vec{b}') + S_{A_2}(\vec{b} - \vec{b}')] } \right\} \right). \quad (5.2) \quad \boxed{\text{CEP2}}$$

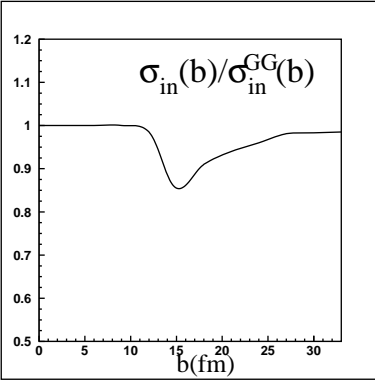


Figure 11: The ratio between the inelastic Au-Au cross sections, calculated from the exact formula, the Glauber-Gribov eikonal approach, as a function of the impact parameter (b).

σ_{tot}^{NN} and σ_{in}^{NN} are the total and inelastic nucleon-nucleon cross sections. Note that the two sets of nucleus-nucleus cross section calculations are only mildly different. A slightly larger local difference is observed in a restricted region of higher impact parameters. Indeed, for $b \ll R_A$ the partial amplitude for nucleus-nucleus scattering in either the Glauber-Gribov approach or in Eq. (5.1)^{CEP1} and Eq. (5.2)^{CEP2}, is very close to 1. At large values of b , Eq. (5.1)^{CEP1} and Eq. (5.2)^{CEP2}, as well as the corresponding Glauber-Gribov cross sections, approach the same limit. A small difference between the two approaches we have studied may, be detected only at $b \approx 2 R_A$ (see Fig. 11)^{ratst}. Note, in addition, that the contribution to the inelastic cross section in this region of b is very small (about 2% at RHIC energies).

Our results suggest that sensitive observables in nucleus-nucleus collision are the number of participants and the nuclear modification factor (NMF). It is well known, that the number of participants N_{part} for $A_1 - A_2$ scattering is equal to

$$N_{part}(b) = \frac{A_1 \sigma_{in}^{A_2}(b) + A_2 \sigma_{in}^{A_1}(b)}{\sigma_{in}^{A_1 A_2}(b)}, \quad (5.3) \quad \boxed{\text{CEP3}}$$

where $\sigma_{in}^{A_i}$ are given by Eq. (3.4)^{HA3} and $\sigma_{in}^{A_1 A_2}(b)$ by Eq. (5.2)^{CEP2}. For Au-Au collisions at RHIC energies ($\sqrt{s} = 200$ GeV), the $b = 0$ ratio $\frac{N_{part}(b)}{N_{part}^{GG}(b)} = 0.93$ with $g G_3 P / \Delta P$ obtained from Ref. [11]^{GLMM}. In this estimate we take $\sigma_{in}^{NN} = \sigma_{tot}^{NN} - \sigma_{el}^{NN} = 42$ mb and for $S_A(b)$ we use the Wood-Saxon parameterization [25]^{WS},

$$S_A(b) = \int_{-\infty}^{+\infty} dz \frac{\rho_0}{1 + e^{\frac{\sqrt{z^2 + b^2} - R_A}{h}}}, \quad (5.4) \quad \boxed{\text{CEP4}}$$

with $\rho_0 = 0.171 \text{ 1/fm}^3$, $R_A = 6.39 \text{ fm}$ and $h = 0.53 \text{ fm}$ for Au. In this calculation we took $\sigma_{in}^{NN} = \sigma_{tot}^{NN} - \sigma_{el}^{NN} - \sigma_{diff}^{NN} = 36 \text{ mb}$. Note that, $\sigma_{diff}^{NN} = 2\sigma_{sd}^{NN} + \sigma_{dd}^{NN}$. The above estimate is more reasonable than the qualitative estimate of 42 mb quoted earlier (see Ref. [26]). N_{coll}^{GG} has been taken from Ref. [KHNA]. We obtain $N_{part}(b=0)/N_{part}^{GG}(b) = 0.90$.

The NMF is defined as

$$R_{AA} = \frac{\frac{d^2\sigma_{A_1A_2}}{dyd^2p_\perp}}{\frac{d^2\sigma_{NN}}{dyd^2p_\perp}} = \frac{1}{N_{coll}} \frac{\frac{d^2N_{A_1A_2}}{dyd^2p_\perp}}{\frac{d^2N_{NN}}{dyd^2p_\perp}}, \quad (5.5) \quad \boxed{\text{NMF}}$$

where N is the hadron multiplicity. In the last equation both $\frac{d^2N_{A_1A_2}}{dyd^2p_\perp}$ and $\frac{d^2N_{NN}}{dyd^2p_\perp}$ are measured experimentally, while the number of collisions defined as $N_{coll} = A\sigma_{in}^{NN}/\sigma_{in}^{A_1A_2}$ has to be calculated. As we have observed for the case of a nucleus-nucleus collision, the Glauber-Gribov approach to N_{coll} gives the same result as the correct formulae, Eq. (5.1)^{CEP1} and Eq. (5.2)^{CEP2}.

Using Eq. (4.6)^{MF5} and Eq. (4.7)^{MF6} we calculate the value of R_{AA} ,

$$R_{AA} = \left(\int d^2b \frac{S_{A_1}(b)}{1 + \tilde{g} G_{enh}(Y/2 - y) S_{A_1}(b)} \right) \left(\int d^2b \frac{S_{A_2}(b)}{1 + \tilde{g} G_{enh}(Y/2 + y) S_{A_2}(b)} \right). \quad (5.6) \quad \boxed{\text{NMF1}}$$

In Table 1 we display the estimates of R_{AA} for Au-Au collisions, calculated in the approach of Ref. [GLMM]. In this approach the contribution of the triple Pomeron interactions are relatively small, leading to a $1 - 2 \text{ mb}$ contribution, which is just a fraction of the calculated single inclusive diffractive cross section. In the above, $\tilde{g}G_{3P}/\Delta_P = n\tilde{g}\gamma$ ($n=1,2,3$) and $\gamma = \gamma_0$ is the value obtained from the data analysis of the

γ/y	0	0	1	2	3	4
	inclusive	centrality 0 – 10%				
γ_0	0.61	0.59	0.60	0.57	0.52	0.46
$2 \gamma_0$	0.42	0.39	0.41	0.385	0.345	0.30
$3 \gamma_0$	0.31	0.28	0.305	0.28	0.25	0.218

Table 1: Inclusive R_{AA} for Au-Au collisions at $W = 200 \text{ GeV}$.

proton-proton scattering in Ref. [GLMM]. $Y = \ln(s/s_0)$ and $s = W^2$, where W denotes the center mass energy. Recall that R_{AA} does not depend on p_\perp . However, we can trust our approach only at small values of p_\perp .

In Table 1 we checked the single diffraction cross sections initiated by triple Pomeron interactions corresponding to γ values ranging from γ_0 , obtained in Ref. [GLMM], to $3\gamma_0$. Fitting the data with γ fixed at either of these values we conclude that the variance of the overall $\chi^2/d.o.f.$ we have obtained is not large. i.e. the data is not very sensitive to the value of γ within the above range. We believe, therefore, that the estimates presented in the Table 1 are instructive for obtaining an approximate value of $R_{A,A}$. For NMF at fixed centrality we have used Ref. [KHNA] relations between the centrality cuts and the essential impact parameter region. Note that the corrections to N_{coll} using the correct formula are small. One can see from Table 1 that R_{AA} , in the centrality region (0 – 10%), is only slightly suppressed in comparison to the inclusive NMF (see also Eq. (5.5)^{NMF}).

In Fig. 12 we plot the data for inclusive R_{AA} (see Refs. [28–31]) as compared with our predictions for $W = 200 \text{ GeV}$. We checked two values of the triple Pomeron vertex: one which, is taken from Ref. [1] ($\gamma = \gamma_0$), and the second is 3 times larger. There are two different interpretations of the physical meaning of our results:

- 1) A traditional one, in which Pomeron calculus is responsible for the structure of the initial partonic wave function of the fast hadron, and/or nucleus. Therefore, we need to divide the experimental values of R_{AA} by the calculated NMF, and explain this ratio $R_{AA}^{exp}/R_{AA}^{theory}$ by accounting for the final state interactions such as jet quenching, energy losses and so on [35, 36].
- 2) In the interpretation which we follow, the Pomeron calculus initiates the Color Glass Condensates [4–6] in the region of large distances. In this case, it gives the correct normalization of R_{AA} in the region of small $p_\perp \ll Q_s$. Q_s is the saturation momentum. The ratio $R_{AA}^{exp}/R_{AA}^{theory}$ can be interpreted as originating from two possible sources: a proper account of the transverse momentum structure of the parton densities in the saturation region (see Refs. [27, 32, 33]), and/or the final state interactions [35, 36].

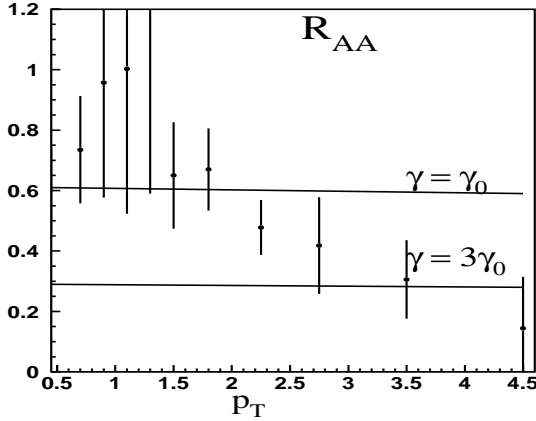


Figure 12: The experimental value of the R_{AA} (the data are taken from Ref. [31]) at $W = 200 \text{ GeV}$. The horizontal lines correspond to two different values of the triple Pomeron vertex. The value of γ_0 as well as other parameters such as \tilde{g} is taken from Ref. [1].

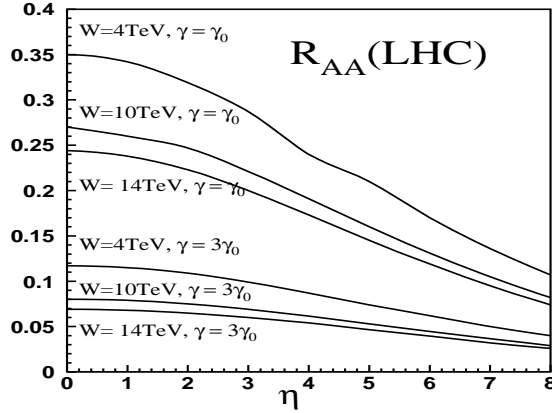


Figure 13: The prediction for the inclusive R_{AA} at the LHC energies. The value of γ_0 as well as other parameters such as \tilde{g} is taken from Ref. [1].

5.2 Hadron-nucleus collisions

The NMF for proton-nucleus collision is defined by the same expression as for nucleus-nucleus,

$$R_{pA} = \frac{\frac{d^2 \sigma_{pA}}{dy d^2 p_\perp}}{\frac{d^2 \sigma_{pp}}{dy d^2 p_\perp}} = \frac{1}{N_{coll}} \frac{\frac{d^2 N_{pA}}{dy d^2 p_\perp}}{\frac{d^2 N_{pp}}{dy d^2 p_\perp}}. \quad (5.7) \quad \text{NMF3}$$

γY	$N_{coll}^{theory}/N_{coll}^{GG}$	0	1	2	3	4	5
γ_0	0.9	0.71	0.66	0.60	0.53	0.46	0.39
$2\gamma_0$	0.81	0.53	0.495	0.44	0.38	0.32	0.26
$3\gamma_0$	0.73	0.415	0.36	0.30	0.25	0.20	0.16

Table 2: $N_{coll}^{theory}/N_{coll}^{GG}$ and $R_{pA}^{eff}(Y) \equiv R_{pA}(Y, y) N_{pA}^{theory}/N_{pA}^{GG}$ as function of rapidity for different values of G_{3P} .

This ratio can be calculated from Eq. (4.7) which lead to the following equation

$$R_{pA}(Y, y) = \frac{\frac{d^2 \sigma_{pA}}{dy d^2 p_{\perp}}}{\frac{d^2 \sigma_{pp}}{dy d^2 p_{\perp}}} = \int d^2 b \frac{\tilde{g} G_{enh}(y) S_A(\vec{b})}{1 + \tilde{g} G_{enh}(y) S_A(\vec{b})}, \quad (5.8) \quad \text{MNF4}$$

where $Y = \ln(s/s_0)$ and y denotes the rapidity of a produced particle. However, N_{coll} for proton-nucleus scattering turns out to be different from the Glauber-Gribov approach estimates that have been used by the experimentalists. It means that we have to calculate

$$R_{pA}^{eff}(Y) \equiv R_{pA}(Y, y) N_{pA}^{theory}/N_{pA}^{GG}, \quad (5.9)$$

where

$$N_{pA}^{theory}(Y) = A \frac{\sigma_{in}^{pp}}{\int d^2 b \frac{\tilde{g} G_{enh}(Y) S_A(\vec{b})}{1 + \tilde{g} G_{enh}(Y) S_A(\vec{b})}}. \quad (5.10) \quad \text{MNF4}$$

For RHIC energy range we can replace $N_{pA}^{theory}/N_{pA}^{GG}$ by $\sigma_{in}^{PP}(\text{theory})/\sigma_{in}^{PP}$. As we saw, a common approximation [27], $\sigma_{in}^{pp}(GG) = \sigma_{tot} - \sigma_{el} = 42 \text{ mb}$, in Glauber-Gribov approach calculations is improved by [26] $\sigma_{in}^{pp}(\text{theory}) = \sigma_{tot} - \sigma_{el} - \sigma_{diff}(GW) = 36 \text{ mb}$, which is suitable for the approach of Ref. [11]. Recall that $\sigma_{diff} = 2\sigma_{sd} + \sigma_{DD}$. GW denotes a contribution initiated by the Good-Walker mechanism, see Ref. [11] for details and references. This difference induces a correcting coefficient $N_{pA}^{theory}/N_{pA}^{GG} = 36/42 = 0.86$. However, in the framework of our approach we need to modify the total and quasi-elastic cross sections due to the interaction with a nucleus rather than a nucleon (see Fig. 14). The correct inclusion of this interaction leads to

$$\sigma_{in}(p + A; Y) = \int d^2 b \left(1 - \exp \left(- \left\{ \sigma_{tot}^{pp} \frac{S_A(b)}{(1 + \tilde{g} G_{enh}(Y) S_A(b))} - (\sigma_{el}^{pp} + \sigma_{diff}^{pp}) \frac{S_A(b)}{(1 + \tilde{g} G_{enh}(Y) S_A(b))^2} \right\} \right) \right). \quad (5.11) \quad \text{MNF5}$$

Table 2 presents our calculations for $N_{coll}^{theory}/N_{coll}^{GG}$. As we have discussed, we can only trust these estimates at low transverse momenta. Comparing $R_{pA}^{eff}(Y)$ with the experimental data (see Ref. [29]), one can see that we reproduce the low transverse momenta data well. As in the case of nucleus-nucleus scattering, we believe that our estimates give the correct normalization for the NMF at low p_{\perp} , leaving the explanation of the p_{\perp} dependence of R_{pA} to the dependence of the parton densities in the saturation region and beyond (see Ref. [33]), and the jet quenching and energy loss in the final state [35, 36]. If we divide all data by our calculated R_{pA}^{eff} , the p_{\perp} dependence of the NMF resembles the ordinary Cronin effect [34] which approaches unity at large p_{\perp} .

6. Conclusions

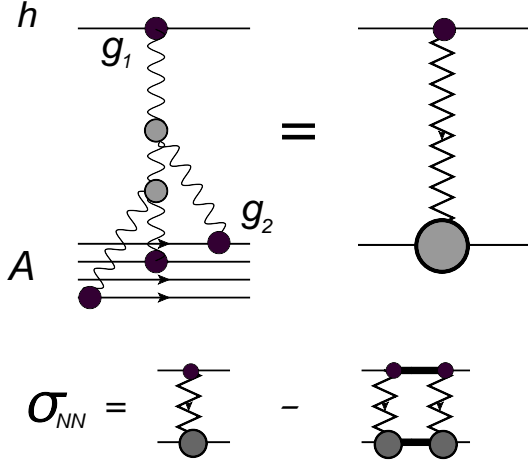


Figure 14: The modified nucleon-nucleon inelastic cross section in our approach.

There are two alternative points of view on this subject. In the traditional one, the soft Pomeron is a separate issue. The estimates based on soft Pomeron approach provides the information on the partonic wave function in the initial state. Therefore, in such an approach, the difference between the experimental data and our estimates should be explained by the interactions in the final state. We support the second point of view in which the soft Pomeron approach that has been developed in this paper and in Ref. [1], is a natural generalization of the Color Glass Condensate approach, and it provides the normalization of the NMF at long distances. Indeed, in CGC approach the relation between $N_{part} = cS_{\perp}Q_s^2$ enters with the coefficient c which could only be determined from numerical simulation. We firmly believe that our approach suggests an alternative method to determine the numerics of CGC. The p_{\perp} dependence within this interpretation, is correlated with the p_{\perp} dependence of the partonic densities in the saturation region and beyond. It depends, as well, on the final state interactions, where we predict only a slight suppression.

Using our approach we predict the NMF at LHC energies and we hope that this prediction will be useful for ion-ion interactions at the LHC.

References

- [1] E. Gotsman, E. Levin, U. Maor and J.S. Miller, *Eur. Phys. J.* **C57** (2008) 689 [arXiv:0805.2799 [hep-ph]]; "Soft interactions at high energies: QCD motivated model", arXiv:0901.1540 [hep-ph]; "The phenomenology of Pomeron enhancement", arXiv:0903.0247 [hep-ph].
- [2] E.A. Kuraev, L.N. Lipatov, and F.S. Fadin, *Sov. Phys. JETP* **45** (1977) 199; Ya.Ya. Balitsky and L. N. Lipatov, *Sov. J. Nucl. Phys.* **28** (1978) 22.
- [3] L.N. Lipatov, *Phys. Rep.* **286** (1997) 131; *Sov. Phys. JETP* **63** (1986) 904 and references therein.

- [GLR] [4] L.V. Gribov, E.M. Levin and M.G. Ryskin, *Phys. Rep.* **100** (1983) 1.
- [MUQI] [5] A.H. Mueller and J. Qiu, *Nucl. Phys.* **B268** (1986) 427.
- [MV] [6] L. McLerran and R. Venugopalan, *Phys. Rev.* **D49** (1994) 2233; 3352; **D50** (1994) 2225; **D53** (1996) 458; **D59** (1999) 09400.
- [B] [7] I. Balitsky, [arXiv:hep-ph/9509348]; *Phys. Rev.* **D60** (1999) 014020 [arXiv:hep-ph/9812311].
- [K] [8] Y.V. Kovchegov, *Phys. Rev.* **D60** (1999) 034008 [arXiv:hep-ph/9901281].
- [MWLK] [9] J. Jalilian-Marian, A. Kovner, A. Leonidov and H. Weigert, *Phys. Rev.* **D59** (1999) 014014 [arXiv:hep-ph/9706377]; *Nucl. Phys.* **B504** (1997) 415 [arXiv:hep-ph/9701284]; J. Jalilian-Marian, A. Kovner and H. Weigert, *Phys. Rev.* **D59** (1999) 014015 [arXiv:hep-ph/9709432]; A. Kovner, J.G. Milhano and H. Weigert, *Phys. Rev.* **D62**, 114005 (2000) [arXiv:hep-ph/0004014]; E. Iancu, A. Leonidov and L.D. McLerran, *Phys. Lett.* **B510** (2001) 133 [arXiv:hep-ph/0102009]; *Nucl. Phys.* **A692** (2001) 583 [arXiv:hep-ph/0011241]; E. Ferreira, E. Iancu, A. Leonidov and L. McLerran, *Nucl. Phys.* **A703** (2002) 489 [arXiv:hep-ph/0109115]; H. Weigert, *Nucl. Phys.* **A703**, (2002) 823 (2002) [arXiv:hep-ph/0004044].
- [RIBRT] [10] V.N. Gribov, *Sov. Phys. JETP* **26** (1968) 414 [*Zh. Eksp. Teor. Fiz.* **53** (1967) 654].
- [SCHW] [11] A. Schwimmer, *Nucl. Phys.* **B94** (1975) 445.
- [BGLM] [12] S. Bondarenko, E. Gotsman, E. Levin and U. Maor, *Nucl. Phys.* **A683** (2001) 649 [arXiv:hep-ph/0001260].
- [COL] [13] P.D.B. Collins, "An introduction to Regge theory and high energy physics", Cambridge University Press 1977.
- [SOFT] [14] Luca Caneschi (editor), "Regge Theory of Low- p_T Hadronic Interaction", North-Holland 1989.
- [LEREG] [15] E. Levin, "An introduction to Pomerons", arXiv:hep-ph/9808486; "Everything about Reggeons. I: Reggeons in 'soft' interaction", arXiv:hep-ph/9710546.
- [GLAUB] [16] R.J. Glauber, "Lectures in Theoretical Physics", edited by W. E. Britten et al. (Interscience, New York) **1**, (1959) 315.
- [GRIBA] [17] V.N. Gribov, *Sov. Phys. JETP* **29** 483 [*Zh. Eksp. Teor. Fiz.* **56** 892 (1969)]; *Sov. Phys. JETP* **30** 709 [*Zh. Eksp. Teor. Fiz.* **57** (1969) 1306].
- [MPSI] [18] A.H. Mueller and B. Patel, *Nucl. Phys.* **B425** (1994) 471; A.H. Mueller and G.P. Salam, *Nucl. Phys.* **B475**, (1996) 293 [arXiv:hep-ph/9605302]; G.P. Salam, *Nucl. Phys.* **B461** (1996) 512; E. Iancu and A.H. Mueller, *Nucl. Phys.* **A730** (2004) 460 [arXiv:hep-ph/0308315]; 494 [arXiv:hep-ph/0309276].
- [LMP] [19] E. Levin, J. Miller and A. Prygarin, *Nucl. Phys.* **A806** (2008) 245 [arXiv:0706.2944 [hep-ph]].
- [RY] [20] I. Gradstein and I. Ryzhik, "Tables of Series, Products, and Integrals", Verlag MIR, Moscow, 1981.
- [GW] [21] M.L. Good and W.D. Walker, *Phys. Rev.* **120** (1960) 1857.
- [BORY] [22] K.G. Boreskov, A.B. Kaidalov, V.A. Khoze, A.D. Martin and M.G. Ryskin, *Eur. Phys. J.* **C44** (2005) 523 [arXiv:hep-ph/0506211].
- [AGK] [23] V.A. Abramovsky, V.N. Gribov and O.V. Kancheli, *Yad. Fiz.* **18** (1973) 595 [*Sov. J. Nucl. Phys.* **18** (1974) 308].
- [MUDI] [24] A.H. Mueller, *Phys. Rev.* **D2** (1970) 2963.

- [WS] [25] C. W. De Jagier, H. De Vries, and C. De Vries, *Atomic Data and Nuclear Data Tables*, **Vol.14 No. 5,6** (1974) 479.
- [KOP] [26] B.Z. Kopeliovich, *Phys. Rev.* **C68** (2003) 044906 [arXiv:nucl-th/0306044]; B.Z. Kopeliovich, I.K Potashnikova and I. Schmidt, *Phys. Rev.* **C73** (2006) 034901 [arXiv:hep-ph/0508277].
- [KHNA] [27] D. Kharzeev and M. Nardi, *Phys. Lett.* **B507** (2001) 121 [arXiv:nucl-th/0012025].
- [AHMS0] [28] I. Arsene *et al.* [BRAHMS Collaboration], *Phys. Rev. Lett.* **91** (2003) 07305.
- [AHMS1] [29] I. Arsene *et al.* [BRAHMS Collaboration], *Phys. Rev. Lett.* **93** (2004) 242303 [arXiv:nucl-ex/0403005].
- [AHMS2] [30] I. Arsene *et al.* [BRAHMS Collaboration], *Phys. Lett.* **B650** (2007) 219 [arXiv:nucl-ex/0610021].
- [ENIX1] [31] S.S. Adler *et al.* [PHENIX Collaboration], *Phys. Rev. Lett.* **96** (2006) 032301 [arXiv:nucl-ex/0510047].
- [KLN] [32] D. Kharzeev, E. Levin and M. Nardi, *Nucl. Phys.* **A747** (2005) 609 [arXiv:hep-ph/0408050]; *Nucl. Phys.* **A730** (2004) 448 [Erratum-ibid. **A743** (2004) 329] [arXiv:hep-ph/0212316]; *Phys. Rev.* **C71** (2005) 054903 [arXiv:hep-ph/0111315]; D. Kharzeev, E. Levin and L. McLerran, *Phys. Lett.* **B561** (2003) 93 [arXiv:hep-ph/0210332].
- [KKT] [33] D. Kharzeev, Y.V. Kovchegov and K. Tuchin, *Phys. Lett.* **B599** (2004) 23 [arXiv:hep-ph/0405045];
- [ronin] [34] J.W. Cronin, *Phys. Rev.* **D68** (2003) 094013 [arXiv:hep-ph/0307037].
- [ELOSS] [35] M. Gyulassy, I. Vitev, X.N. Wang and B.W. Zhang, *Quark Gluon Plasma* **3** (2003) 123, editors: R.C. Hwa and X.N. Wang, World Scientific, Singapore, [arXiv:nucl-th/0302077]; I. Vitev, *Phys. Lett.* **B562** (2003) 36 [arXiv:nucl-th/0302002]; M. Gyulassy, P. Levai and I. Vitev, *Nucl. Phys.* **B594** (2001) 371 [arXiv:nucl-th/0006010]; *Phys. Rev. Lett.* **85** (2000) 5535 [arXiv:nucl-th/0005032].
- [BDMS] [36] R. Baier, A. H. Mueller, D.T. Son and D. Schiff, *Nucl. Phys.* **A698** (2002) 217; R. Baier, Y.L. Dokshitzer, A.H. Mueller and D. Schiff, *JHEP* **0109** (2001) 033 [arXiv:hep-ph/0106347]; *Phys. Rev.* **C60** (1999) 064902 [arXiv:hep-ph/9907267]; *Nucl. Phys.* **B531** (1998) 403 [arXiv:hep-ph/9804212]; *Nucl. Phys.* **B484** (1997) 265 [arXiv:hep-ph/9608322]; *Nucl. Phys.* **B483** (1997) 291 [arXiv:hep-ph/9607355].
- [ronin] [37] J.L. Albacete, N. Armesto, A. Kovner, C.A. Salgado and U.A. Wiedemann, *Phys. Rev. Lett.* **92** (2004) 082001 [arXiv:hep-ph/0307179]; E. Iancu, K. Itakura and D.N. Triantafyllopoulos, *Nucl. Phys.* **A742** (2004) 182 [arXiv:hep-ph/0403103]; R. Baier, A. Kovner and U.A. Wiedemann, *Phys. Rev.* **D68** (2003) 054009 [arXiv:hep-ph/0305265].